NeuroImage: Clinical 29 (2021) 102555

Contents lists available at ScienceDirect

NeuroImage: Clinical

journal homepage: www.elsevier.com/locate/ynicl

Diffusion kurtosis imaging detects subclinical white matter abnormalities in Phenylketonuria

Sarah C. Hellewell [a,1], Thomas Welton [a,1], Kate Eisenhuth [b], Michel C. Tchan [b,c], Stuart M. Grieve [a,d,*]

[a] Imaging and Phenotyping Laboratory, Charles Perkins Centre, Faculty of Medicine and Health, University of Sydney, NSW, 2006, Australia
[b] Department of Genetic Medicine, Westmead Hospital, Westmead, NSW, 2145, Australia
[c] Sydney Medical School, University of Sydney, Camperdown, NSW, 2050, Australia
[d] Department of Radiology, Royal Prince Alfred Hospital, Camperdown, Sydney, NSW, 2050, Australia

ARTICLE INFO

Keywords:
Diffusion kurtosis imaging
DKI
Phenylketonuria
PKU
White matter pathology

ABSTRACT

Objective: Phenylketonuria (PKU) is an autosomal recessive disorder whereby deficiencies in phenylalanine metabolism cause progressive neurological dysfunction. Managing PKU is challenging, with disease monitoring focussed on short-term phenylalanine control rather than measures of neuronal damage. Conventional imaging lacks sensitivity, however diffusion kurtosis imaging (DKI), a new MRI method may reveal subclinical white matter structural changes in PKU.

Methods: This cohort study involved adults with PKU recruited during routine clinical care. MRI, neurocognitive assessment and historical phenylalanine (Phe) levels were collected. A hypothesis-generating case study comparing diet-compliant and non-compliant siblings confirmed that DKI metrics are sensitive to dietary adherence and prompted a candidate metric (K_{rad}/K_{FA} ratio). We then tested this metric in a Replication cohort (PKU = 20; controls = 43).

Results: Both siblings scored outside the range of controls for all DKI-based metrics, with severe changes in the periventricular white matter and a gradient of severity toward the cortex. K_{rad}/K_{FA} provided clear separation by diagnosis in the Replication cohort ($p < 0.001$ in periventricular, deep and pericortical compartments). The ratio also correlated negatively with attention ($r = -0.51$ & -0.50, $p < 0.05$) and positively with 3-year mean Phe ($r = 0.45$ & 0.58, $p < 0.01$).

Conclusion: DKI reveals regionally-specific, progressive abnormalities of brain diffusion characteristics in PKU, even in the absence of conspicuous clinical signs or abnormalities on conventional MRI. A DKI-based marker derived from these scores (K_{rad}/K_{FA} ratio) was sensitive to cognitive impairment and PKU control over the medium term and may provide a meaningful subclinical biomarker of end-organ damage.

1. Introduction

Phenylketonuria (PKU) is a genetic disorder of amino acid metabolism. Untreated PKU results in intellectual impairment due to neurotoxic effects of accumulated phenylalanine (Phe) (Williams et al., 2008). Blood Phe is the only biomarker to guide management, however Phe concentration is an inconsistent predictor of changes in neurocognitive function during adulthood (Romani et al., 2017, 2019; Hofman et al., 2018). The classic radiological appearance of PKU is of bilateral white matter (WM) changes, although this is non-specific and only consistently seen in poorly-controlled disease, rendering it unsuitable for use in patient management. Diffusion kurtosis imaging (DKI) is a novel analysis for diffusion imaging data, reflecting subtle changes in brain parenchymal structure (Arab et al., 2018). DKI extends standard diffusion tensor imaging by accounting for non-Gaussian diffusion, permitting detection of sub-voxel alterations in parenchyma (Hansen and Jespersen, 2016). We investigated the potential of DKI as a measure of subclinical WM neuropathology in PKU.

* Corresponding author at: Sydney Translational Imaging Laboratory, Heart Research Institute, Sydney Medical School & Charles Perkins Centre, University of Sydney, Camperdown, NSW, 2006, Australia.
E-mail address: stuart.grieve@sydney.edu.au (S.M. Grieve).
[1] Authors contributed equally.

https://doi.org/10.1016/j.nicl.2020.102555
Received 17 July 2020; Received in revised form 2 December 2020; Accepted 29 December 2020
Available online 9 January 2021

PKU is managed with a strict low-protein diet, with non-compliance leading to elevated Phe concentration and downstream negative neurocognitive consequences (Enns et al., 2010; Christ et al., 2010; Huijbregts et al., 2002; Trefz et al., 2015). Historically, the protein-restricted diet was ceased in early teenage years but is now lifelong due to evidence of ongoing neurological dysfunction in adults with elevated Phe (Romani et al., 2017; Hofman et al., 2018; Nardecchia et al., 2015; Weglage et al., 2013). The dominant clinical neuroimaging findings in poorly-controlled PKU are periventricular WM hyperintensities radiating toward the cortex, suggesting progressive and regionally-selective pathobiology (Pearsen et al., 1990; Ullrich et al., 1994; Bick et al., 1993). While this "textbook" PKU appearance is detectable in advanced disease, early changes are subtle, limiting the use of clinical imaging in day-to-day management.

Several PKU studies have employed conventional diffusion-tensor imaging (DTI), demonstrating lowered diffusivity in the WM (Leuzzi et al., 2007) correlating with elevated Phe and cognitive dysfunction (Dezortova et al., 2001; Ding et al., 2008; Vermathen et al., 2007; González et al., 2018; Antenor-Dorsey et al., 2013; Kakulas et al., 1968). These changes likely reflect developmental hypomyelination and progressive demyelination, with post-mortem myelin breakdown products (Malamud, 1966; Falangola et al., 2014). Recent studies demonstrate that DKI may delineate WM pathology, particularly in the setting of demyelinating diseases (Maller et al., 2019). DKI measures the kurtosis of the diffusion distribution within a voxel, with changes in microstructural architecture captured using different kurtosis metrics (Arab et al., 2018; Malamud, 1966). In this way, greater kurtosis values can be conceptualised as representative of higher deviation of water molecules from an 'expected' pattern, reflecting a normal restricted tissue environment (Arab et al., 2018).

We initially report DKI findings in a hypothesis-generating case study of two siblings with PKU. Based on these observations we defined a DKI metric sensitive to dietary compliance, then performed a Replication analysis in 20 adults with PKU and 43 controls. We hypothesised that: disease severity would correspond to DKI measures of WM pathology; and alterations would occur in a gradient of decreasing severity radiating outward from the periventricular WM (the most prominent area of white mater pathology on neuroimaging); and that a biomarker based on the spatial pattern of these DKI abnormalities would be sensitive to disease status.

2. Materials and methods

2.1. Patients

All patients were prospectively consented and imaged under a common protocol for the Brain Passport Project (Silverstein et al., 2007). The study was conducted under ethics approval from the Western Sydney Local Health District Human Research Ethics Committee, reference number 14/WMEAD22. Written informed consent was obtained from all study participants.

2.2. Sibling case study

Two adults (Patient X, female and Patient Y, male) diagnosed with PKU during routine newborn screening were evaluated via the Adult Genetic Metabolic Disorders Clinic at Westmead Hospital, Sydney, Australia. Healthy control cohorts (11 females, 14 males) were drawn from Brain Passport to match both siblings, recruited as described previously (Silverstein et al., 2007). Controls were also matched for age (±3 years of Patient X/Y), and were cognitively unimpaired across four domains: motor response speed, attention, information processing efficiency and executive function (±2 standard deviations of a normative cohort, n = 40,000[27]). Controls had no history of cardiac, metabolic or genetic disorder, nor history of drug dependence. All were proficient in English and had no contraindication to MRI.

2.3. Replication cohort

Following our analysis of the Sibling Case study, a cohort of 20 adult patients with PKU were imaged using the same protocol, with data processed for DKI analysis. 43 age and sex-matched control subjects were drawn from Brain Passport to match the confirmatory PKU Cohort.

2.4. Clinical data

Dried bloodspot Phe levels were obtained for Patients X and Y and the PKU cohort as part of routine clinical care. Phe levels were not consistently available throughout patients' lifespans due to variable compliance with monitoring. Phe concentrations were calculated as lifetime mean, three year mean, and level at the timepoint closest to imaging.

2.5. Cognitive testing

Computerized neurocognitive testing was performed at the time of imaging using the Brain Resource WebNeuro battery (Jones et al., 1999). PKU and control patients were examined using attention, memory, information processing, executive function and response speed tasks, with scores normalized to the Brain Resource database (Jones et al., 1999).

2.6. Imaging parameters

MRI images were acquired at Sydney Adventist Hospital between October 2016 and November 2018. A 3-Tesla GE Discovery MR750w MRI (GE Healthcare, Milwaukee, WI) with DV25.0 software and 32-channel Nova head coil (Nova Medical, Wilmington, MA) was used as follows: Contiguous sagittal MPRAGE T1-weighted image with prospective motion correction (TR = 8.39 ms, TE = 3.17 ms, TI = 900 ms, flip angle = 8°, matrix = 256x256, 198 slices, voxel dimensions = 1 mm isotropic).

- Multi-shell multi-band diffusion MRI: ~10 min (multiband factor = 3, 66 slices, b-values of 700, 1000, and 2800 mm/s^2, 140 unique gradient directions, TR = 4323 ms, TE = 91.80 ms, flip angle = 90°, matrix = 128x128, voxel dimensions = 2 mm isotropic). This gradient scheme was based on those proposed by Jones et al. (Tabesh et al., 2011), in which data points are evenly distributed over a unit sphere in Q-space. Scanning time was 9 min. A further diffusion-weighted sequence was also acquired with a reversed phase-encoded non-diffusion-weighted (b = 0) volume.
- Sagittal CUBE FLAIR: ~5 min (matrix = 256x256, TR = 6502 ms, TE = 99.76 ms, TI = 1715 ms, flip angle = 90°, voxel dimensions = 1 mm isotropic).
- Sagittal CUBE T2-weighted: ~3 min (matrix = 256x256, TR = 2502 ms, TE = 97.97 ms, flip angle = 90°, voxel dimensions = 1 mm isotropic).
- Axial clinical DWI: ~1 min (matrix = 164x164, TR = 6879 ms, TE = 71.80 ms, flip angle = 90°, voxel dimensions = 1.5x1.5x4.5 mm).
- Acquired but not included in this study: further DTI scans and fMRI. Total scan time was just over 30 min.

2.7. Image analysis

Clinical MRI data was assessed by a neuroradiologist (SMG) to characterise conventional structural brain abnormalities using T1-weighted, T2-weighted, FLAIR and clinical DWI scans.

Multi-band diffusion data were processed using Diffusion Kurtosis Estimator software (Version 1; https://www.nitrc.org/projects/dke/). We obtained maps of axial diffusion (AD), radial diffusion (RD), mean diffusivity (D_{mean}), fractional anisotropy (FA), axial kurtosis (K_{Ax}), radial kurtosis (K_{Rad}), mean kurtosis (K_{mean}) and kurtosis fractional

anisotropy (K_{FA}) with an approximate processing time of one hour per subject. This included a smoothing step with a Gaussian kernel to reduce the impact of noise and mis-registration, estimation of the diffusion (second order) and kurtosis (fourth order) tensors using the CLLS quadratic programming algorithm (Fischl, 2012).

T1-weighted images were automatically segmented into WM, gray matter and CSF binary masks using FreeSurfer 6.0 (Zhang et al., 2001). We then constructed personalised binary masks for periventricular, pericortical and deep WM, incorporating probabilistic and partial volume information from FSL FAST (Greve and Fischl, 2009) for three classes (GM, WM and CSF; Fig. 1) using 4 iterations to estimate the bias field. First, all voxels containing partial volumes were excluded. The WM mask was separated into periventricular, pericortical and deep sections based on its proximity to the ventricles for "periventricular" and proximity to the cortex for "pericortical". The CSF/lateral ventricle mask, and cortical masks were expanded by three voxels in all directions and the volume overlapping the WM mask was labelled correspondingly. The remaining voxels were classed as "deep". Masks were transformed to diffusion space using boundary-based registration between T1-weighted and diffusion images followed by application of the transform (Koch, 1999). This approach is more robust to WM pathology and artefacts since only intensities near the white–grey boundary are used. We confirmed that voxel-wise distributions of diffusion and kurtosis scalars were approximately normal within masks, and then calculated the mean and standard deviation for each.

2.8. Statistical analyses

Statistical analyses were conducted using SPSS (v.25; IBM; Chicago, IL). The Kolmogorov-Smirnov test for normality was applied to examine data distribution within and between groups. Cognitive data (Z-scores), brain volumes and diffusion kurtosis metrics in each of the WM tissue masks for patients with PKU were compared to controls using one-way ANOVAs with post-hoc Tukey test. Pearson's correlation was used to examine relationships between the K_{rad}/K_{FA} ratio, cognition and Phe concentration. Correction for multiple comparison in correlation data was performed using the Benamini-Horchberg procedure.

3. Results

3.1. Sibling case study

Clinical and demographic characteristics are shown in Table 1. Lifetime Phe concentrations for Patients X and Y are presented in Fig. 2 (left panels). Newborn Phe levels were similar (Patient X: 600 μmol/L; Patient Y: 430 μmol/L) and outside normal range of 30–60 μmol/L (Inwood et al., 2017). Their childhood Phe levels were also frequently above the recommended range (120–360 μmol/L) (Hood et al., 2014). Although mean Phe levels were marginally higher in sibling Y, the Index of Dietary Control was not significantly different (584 for sibling Y and 565 for sibling X), indicating that childhood levels of dietary controls were similar (Blau et al., 2010). After age 20 Patient X had stable Phe concentrations in the range of 487 ± 134 μmol/L. In contrast, Patient Y's Phe rose to 1645 ± 165 μmol/L due to poor dietary compliance.

3.2. Cognitive assessment

There were no differences in normalized cognitive scores between male and female control participants (Table 1 & Supplemental data), so sex-based groups were combined for analysis (n = 25). Patient Y

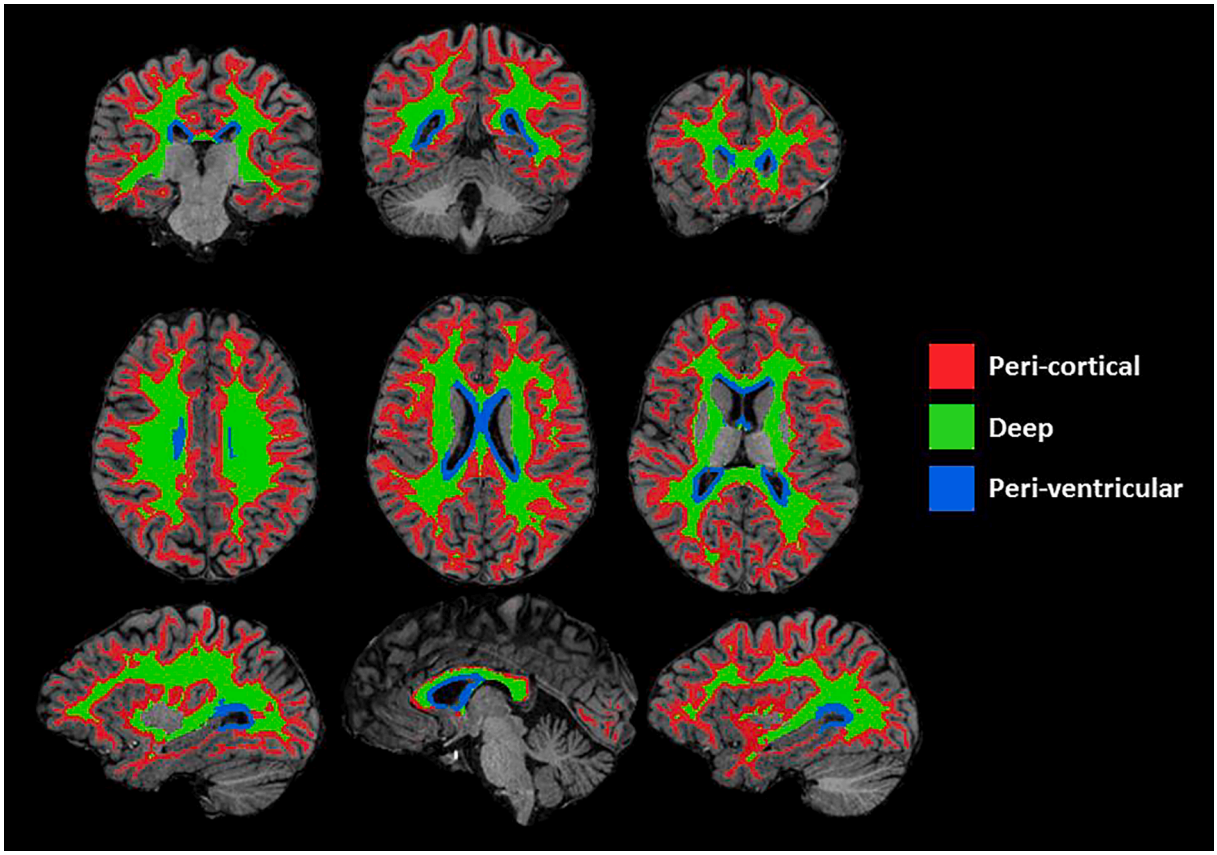

Fig. 1. Example white matter masks. Example masks derived from a control patient, delineating pericortical (red), deep (green) and periventricular white matter (blue) on T1-weighted images. The final masks were eroded to avoid partial volume effects. (For interpretation of the references to colour in this figure legend, the reader is referred to the web version of this article.)

Table 1
Clinical, demographic and neurocognitive characteristics of Patients X, Y and matched control cohorts.

Variable	Patient X	Age-matched Female controls (n = 11)	Patient Y	Age-matched Male controls (n = 14)	PKU cohort (n = 20)	Control cohort (n = 43)
Age (years)	25	23 (2.0)	28	26 (2.6)	36.3 (11.1)	31.9 (13.1)
Height (cm)	153	163.18 (6.13)	177	179.00 (5.20)	168.85 (10.21)	171.35 (9.08)
Weight (kg)	54	60.00 (9.13)	72	83.09 (14.35)	78.60 (19.23)	73.59 (15.57)
Initial Phe level (μmol/L)	600	–	430	–	600	–
Lifetime						
Mean Phe level (SD) (μmol/L)	461 (251)	–	609 (424)	–	491 (348)	–
0–12 years (SD)						
Mean Phe level (SD) (μmol/L)	395 (284)	–	511 (291)	–	–	–
20 + years (SD)						
Mean Phe level (SD) (μmol/L)	487 (134)	–	1645 (165)	–	–	–
Neurocognitive scores						
Response speed Z (SD)	−1.42	0.77 (0.83)	−0.06	0.34 (0.70)	−0.75 (2.19)[b]	0.49 (0.69)
Information processing efficiency Z (SD)	−0.55	0.57 (0.59)	0.032	0.11 (0.84)	−0.64 (1.18)[a]	0.12 (0.70)
Attention Z (SD)	−0.16	−0.10 (0.92)	−1.63	−0.20 (0.73)	−0.66 (1.66)	−0.37 (1.00)
Executive function Z (SD)	0.31	0.47 (0.90)	0.13	0.24 (0.70)	−0.16 (0.94)	0.18 (0.96)

Phe = phenylalanine; PKU = phenylketonuria; SD = standard deviation.
[a] $p < 0.01$, PKU vs. control.
[b] $p < 0.001$, PKU vs. control.

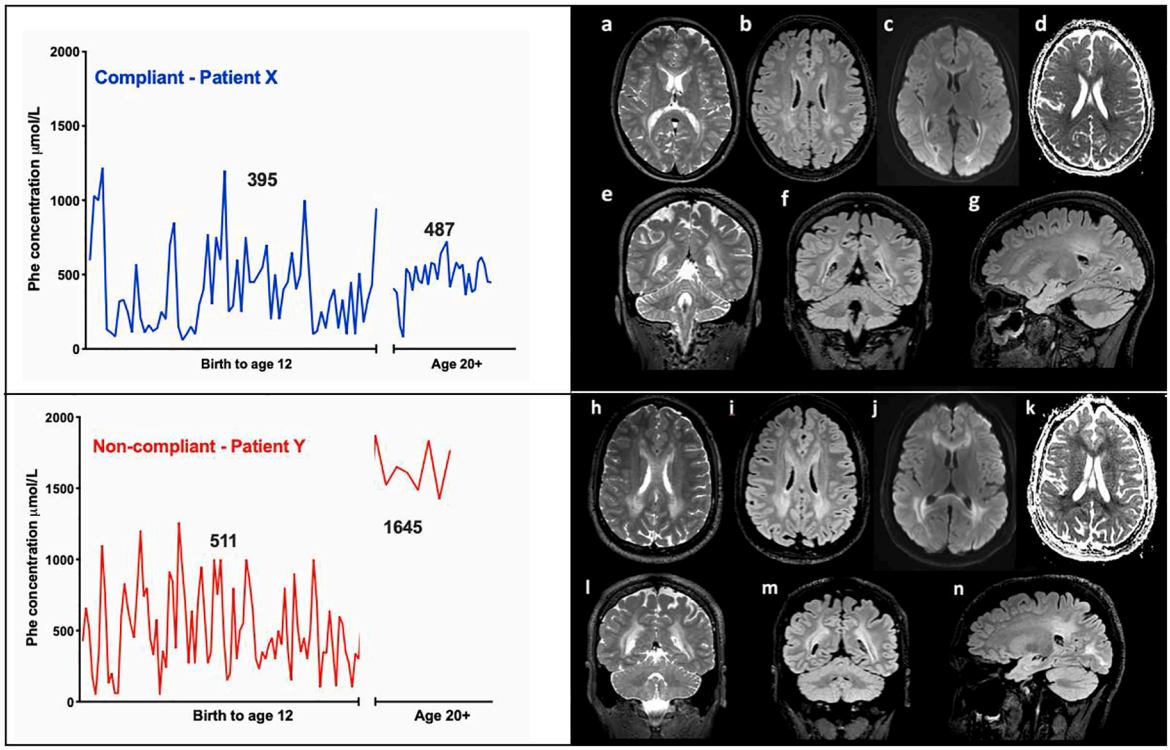

Fig. 2. Comparison of lifetime Phe concentrations and MRI findings for Patient X ("Compliant", top row) and Patient Y ("Non-compliant", bottom row). Phe levels are presented from initial diagnosis at birth to age 12, then around age 20 to the time of imaging. (C) Clinical radiological findings from conventional sequences demonstrate characteristic posterior white matter hyperintensities on T2-weighted (a, e & h, l) and FLAIR (panels b, f, g & I, m, n), together with abnormal diffusion weighted imaging findings (c, d & j, k). Changes were more severe for Patient Y however both show reduced ADC in both frontal and occipital horns of the lateral ventricles and in the parietal white matter.

performed poorly relative to Patient X in most cognitive measures. Both patients demonstrated normal executive function control (±1 SD of control). Patient Y displayed mild deficits in attention (Z = −1.63) relative to control Z-scores, although he was within the normal range for motor response speed and information processing. Patient X had impaired motor response speed compared to control (Z = −1.42), while attention was ± 1 SD of control values.

3.3. Clinical radiological findings

Conventional radiological T2-weighted, FLAIR and diffusion-weighted MRI scans for both patients revealed a periventricular pattern of WM hyperintensities (WMH), most severe proximal to the ventricles with advancement to parieto-occipital regions (Fig. 2). The degree of WM alteration was less pronounced for Patient X (1A-G) than

Patient Y (1H-N). Global brain volumes for patients with PKU and their controls are shown in Table S1. Patient X was ± 1 SD of control for total brain volume (TBV; Z = 0.37), GM (Z = 0.04), WM (Z = 0.73) and CSF (−0.28). Patient Y had smaller volumes compared to age- and sex-matched controls (Z = −1.67, −1.56, −1.38, −2.26 for TBV, GM, WM and CSF respectively).

3.4. Diffusion and diffusion kurtosis imaging: Qualitative findings

Fig. 3 illustrates changes seen in a standard DTI metric (FA) and two DKI metrics (K_{rad}, K_{FA}) for the siblings compared to a representative control. No qualitative changes were seen between PKU siblings and control for FA, with predominantly uniform FA throughout the WM. For the kurtosis measures, PKU siblings showed striking regional periventricular elevations. K_{rad} had a uniform pattern of higher kurtosis compared to controls, radiating smoothly out from the periventricular region toward the cortex. In contrast, K_{FA} was highest in periventricular regions with rapid drop-off compared to controls toward the cortex. For both metrics, elevated periventricular kurtosis was especially profound for Patient Y.

3.5. Diffusion and diffusion kurtosis imaging: Quantitative findings

Diffusion and DKI metrics were normally distributed across controls with no sex-based differences, so were analysed as a single group. Fig. 4 and Table S2 summarise regional measurements of dMRI and kurtosis (Fig. 1), stratifying the WM into periventricular, deep and subcortical divisions.

With the exception of FA, dMRI and DKI in the periventricular region were severely abnormal in the siblings. Most metrics also showed differences in the deep WM, with changes more attenuated in the cortex (Fig. 4A–H). MK in the periventricular WM was 40% higher for Patient Y than controls (Z = 4.15) and 30% higher in Patient X than controls (Z = 2.5). Conversely, MD in the periventricular WM was 37% lower in Patient Y compared to controls (Z = −2.00) and 27% lower in in Patient X compared to controls (Z = −1.30). Diffusion and kurtosis metrics in pericortical WM did not differ with the exception of the K_{FA}, where Patients Y and X scored −1.50 and −1.00 SDs *below* controls, respectively. For metrics showing a group difference (all except FA), in all WM compartments, Patient Y had greater abnormalities compared to Patient X (binomial test for probability of 18 or more out of 24 positive observations: p = 0.01). The largest relative difference between Patients X and Y was K_{Ax} in the deep WM, for which Patient X was particularly abnormal (Z = 4.5) compared to controls, and Patient Y was strikingly abnormal (Z = 13.0).

3.6. Biomarker of WM alteration in PKU: K_{rad} /K_{FA} ratio

Of the diffusion and DKI metrics, K_{rad} and K_{FA} demonstrated the most linear gradients across WM compartments for Patients X and Y, and also the greatest deviation from controls across WM compartments (see Fig. 4D and H). In particular, the *gradient of change* for K_{FA} from the periventricular region radiating outwards was reversed relative to controls, going from *higher* K_{FA} (periventricular) to *lower* K_{FA} (pericortical), compared to changing from *lower to higher* in controls. In contrast, patients and controls showed a similar pattern of spatial change for K_{rad} (a gradient of higher periventricular kurtosis to lower pericortical kurtosis), but the *magnitude of difference* in the periventricular region was particularly large. Based on these findings, we reasoned that subclinical structural changes in PKU might be pragmatically represented by a simple ratio comprising the K_{rad} and K_{FA} metrics: K_{FA} potentially reflecting a gradient of disease severity radiating toward the cortex, and K_{rad} potentially a sensitive marker of early disease. We hypothesised that combining these metrics may increase sensitivity across the three WM segments. In the periventricular and deep WM, this K_{rad}/K_{FA} ratio clearly delineated Patients X and Y from their controls (Fig. 4I). Importantly, discrimination between these two patients with differing PKU severities was also observed in each WM subdivision (particularly the deep WM), with Patient X closer to controls than Patient Y, concordant with historical Phe levels and neurocognitive assessment.

3.7. Clinical characterisation of Replication cohort

Clinical, demographic and neurocognitive characteristics for the PKU Replication cohort and their matched control group are presented in Table 1. No significant sex, age, height or weight differences were present. Cognitive Z-scores were normally distributed both within and between cohorts with the exception of response speed, which did not pass significance when cohorts were combined (but did when assessed separately). Mean Z-scores for the PKU cohort were significantly lower for response speed ($p < 0.001$), and information processing efficiency ($p < 0.01$) compared to control, while attention and executive function were unaffected.

3.7.1. Clinical radiological findings

Radiological examination of T2-weighted, FLAIR and clinical dMRI scans for the Replication PKU cohort were largely unremarkable, with normal-appearing WM for most subjects (86%). TBV was reduced in PKU subjects by 20% (PKU 1464 mL vs. 1618 mL controls; p = 0.004). This was likely driven by a reduction in WM (−10%; p = 0.026) with a preservation of overall gray matter (PKU 657 mL vs 687 mL controls; p = 0.12).

3.8. K_{rad} /K_{FA} ratio in Replication cohort

Fig. 4J depicts the between-group differences in K_{rad} /K_{FA} in the Replication cohort. This ratio was significantly elevated in all WM divisions in PKU patients (Fig. 4J; $p < 0.001$ for all), translating to a 10% increase in K_{rad} /K_{FA} ratio in the periventricular WM and 8% in the deep and pericortical WM in the PKU cohort compared to controls.

3.9. Relationship of K_{rad} /K_{FA} ratio to clinical metrics

No relationship was found between the K_{rad} /K_{FA} ratio in any WM region and mean lifetime Phe (periventricular: (r[20] = 0.09, p = 0.69); deep WM: (r[20] = 0.10, p = 0.68); pericortical: (r[20] = 0.08, p = 0.75). However, the relationship between Phe level and the K_{rad} /K_{FA} ratio was significant for PKU control in the medium term, with positive correlations between the mean Phe level of the previous 3 years (average of 9 Phe samples per patient, range 2 to 39 samples) and K_{rad} /K_{FA} ratio in the periventricular (r[20] = 0.45, p = 0.04) and deep WM (r[20] = 0.58, p = 0.007). After correction for multiple comparisons, these p-values were revised to 0.06 (periventricular WM) and 0.01 (deep WM). This finding was also echoed in the deep WM with Phe level taken closest to the time of MRI (r[20] = 0.51, p = 0.02; corrected p = 0.03).

Finally, we investigated whether the K_{rad} /K_{FA} ratio was related to cognitive function by correlating K_{rad} /K_{FA} ratios and mean cognitive Z-scores. We found negative correlations between attention and the K_{rad} /K_{FA} ratio in the periventricular (r[19] = −0.51, $p < 0.03$) and deep WM (r[19] = −0.49, $p < 0.03$), however this finding did not survive correction for multiple comparisons.

4. Discussion

This is the first study applying DKI in evaluation of PKU. Our research suggests advanced imaging may provide more quantitative and objective tools to elucidate the full extent of pathology and with further investigation may present a tool to guide clinical management. In summary, our findings demonstrate that diffusion and DKI metrics are sensitive to WM abnormalities in the absence of overt structural alteration, and generate additional hypotheses about relationships to Phe levels over time.

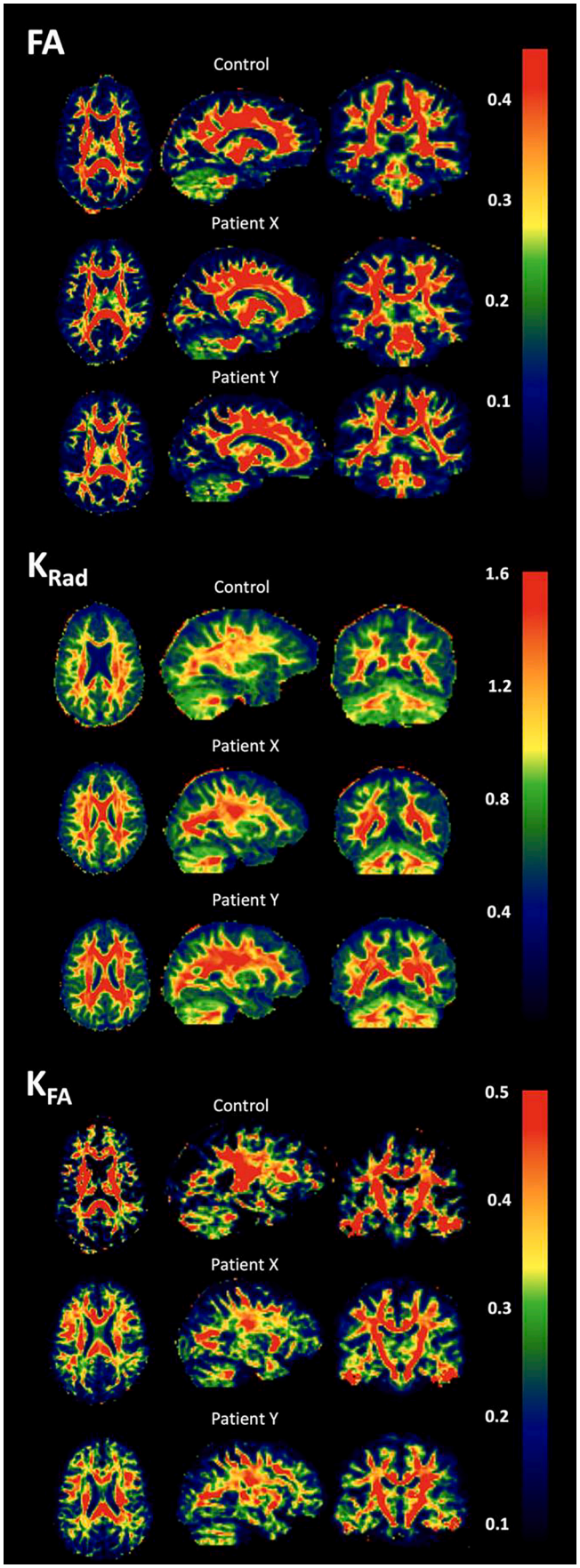

(caption on next column)

Fig. 3. Metric images from a representative control subject, Patient X and patient Y demonstrating selected diffusion (fractional anisotropy (FA), top panel) and DKI (radial kurtosis (K_{rad}), middle panel; kurtosis fractional anisotropy (K_{FA}), bottom panel). While FA was unchanged in PKU siblings, pronounced differences were seen in the kurtosis metrics, with increased severity in Patient Y. Colour bars for each metric are representative of metric scale.

PKU causes progressive, anatomically-specific WM alterations observable on clinical MRI. The literature suggests that modest diet maintenance is insufficient to prevent WM pathology, and that poorer compliance begets imaging abnormalities (Ding et al., 2008). Our study confirms these findings and demonstrates that subclinical WM damage can be detected via dMRI/DKI, even in the absence of conspicuous clinical manifestations.

Siblings X and Y had similar Phe during childhood and adolescence and experienced similar environments; therefore differences in WM pathology likely occurred during adulthood. We predicted that the diet-compliant sibling with lower adult Phe levels would have comparatively preserved WM microstructure, which was the case for all metrics (except FA), although both siblings were dissimilar to controls. Metric size and directions corroborate previous findings showing no change in FA but decreases in MD in early-treated PKU (Leuzzi et al., 2007; Antenor-Dorsey et al., 2013; Kakulas et al., 1968; Steven et al., 2014; Anderson and Leuzzi, 2010). We also proposed that DKI may be superior to tensor-based metrics to measure WM abnormalities. Our findings instead support the concept that DTI and DKI metrics represent fundamentally different microstructural properties (Dyer, 1999), with DKI adding important complementary data that is not available via standard DTI methods. An important consideration of the DTI model is the assumption of a Gaussian distribution, with water movement occurring in an unrestricted environment. In reality, cellular barriers and compartments create a more complex environment, restricting diffusion. As a measurement of deviation from the Gaussian distribution, DKI provides additional information as to the tissue microstructure, detecting anisotropic as well as isotropic diffusion.

The now substantial evidence of WM alteration in PKU has largely been derived from neuroimaging studies (Taylor and Hommes, 1983), with knowledge from clinical post-mortem studies (Kienzle Hagen et al., 2002) and preclinical experimental models of hyperphenylalaninemia suggesting myelin alteration as a prominent factor (Deon et al., 2015). Although the molecular pathological mechanisms of these changes in PKU are unknown, aberrant astrogliosis, oxidative stress (Falangola et al., 2014; Jelescu et al., 2016) and inflammation (Kelm et al., 2016) have been demonstrated in clinical and experimental PKU.

Reflecting the extent of diffusion occurring perpendicular to fibre tracts, D_{rad} has been suggested as a marker of dys- or demyelination, with an inverse relationship to myelin integrity (i.e. higher D_{rad} reflecting decreased integrity) (Arab et al., 2018). Although K_{rad} has been investigated much less frequently compared to D_{rad}, preclinical studies employing electron microscopy to corroborate neuroimaging findings have demonstrated that K_{rad} can be correlated with total axonal water fraction (Chuhutin et al., 2020) and more accurately reflect the myelin content (Hansen, 2019) than traditional DTI metrics. This finding has also been echoed in a preclinical model of multiple sclerosis, in which K_{rad} demonstrated the strongest relationship with disease severity, and was more able to discern subtle changes in normal-appearing white matter (Lesbats et al., 2020). While FA measures the degree of diffusion anisotropy over three directions, it is particularly susceptible to errors in regions of complex tissue microstructure, such as crossing fibres (Hansen and Jespersen, 2016; Zhang et al., 2019). K_{FA} does not suffer such constraints, and more accurately models WM complexity (Hansen and Jespersen, 2016). K_{FA} is a lesser-explored DKI metric, with no preclinical histological validation studies performed to date. However, K_{FA} has been demonstrated as a superior metric in delineating tumor from normal cortical tissue in a preclinical

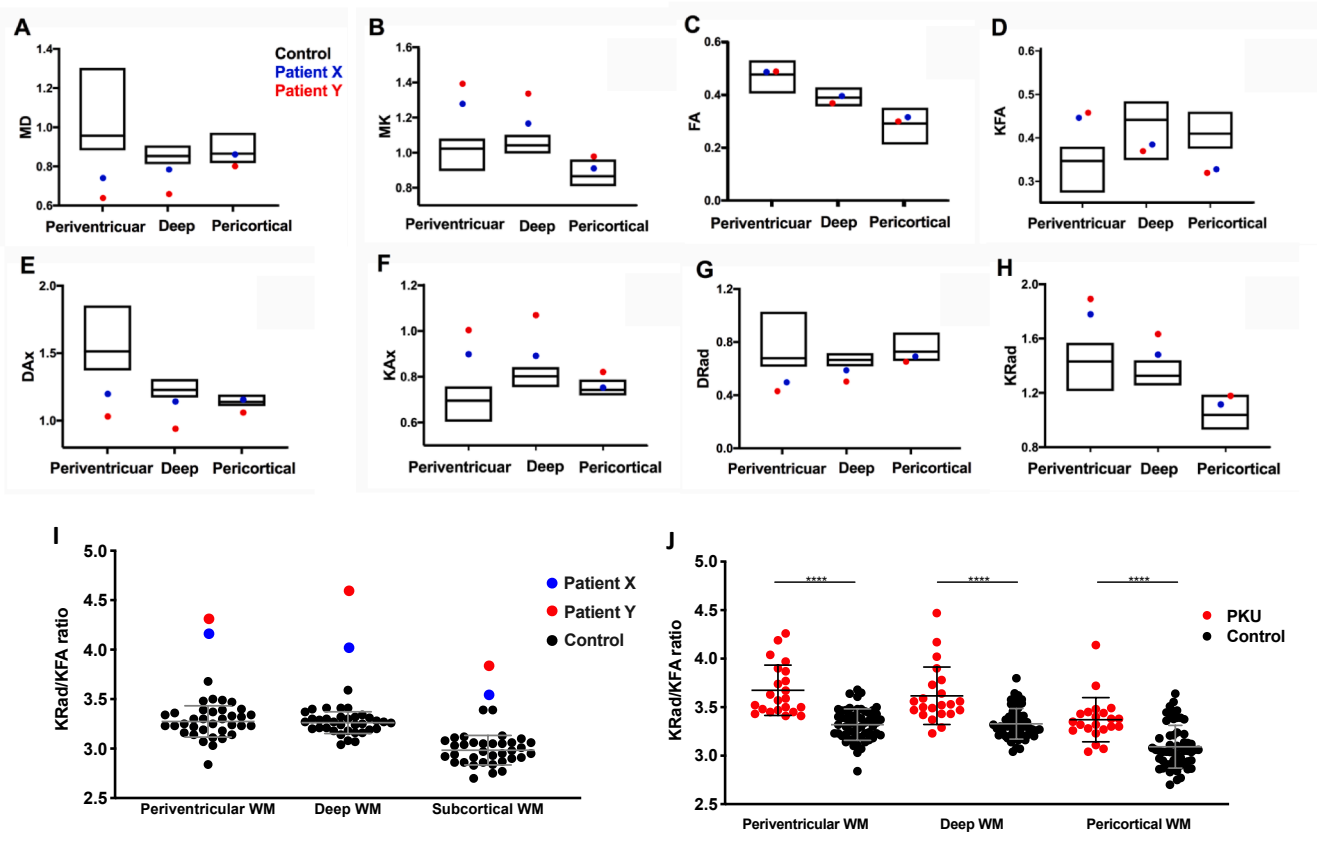

Fig. 4. Diffusion and diffusion kurtosis metrics for the sibling Case study and controls stratified by periventricular, deep and pericortical subdivisions of WM. (A, B) MD (mean diffusivity), MK (mean kurtosis); (C, D) FA (fractional anisotropy), K_{FA} (kurtosis fractional anisotropy); (E, F) D_{ax} (axial diffusivity) K_{ax} (axial kurtosis); (G, H) D_{rad} (radial diffusivity), K_{rad} (radial kurtosis). For A-H, the matched control cohort is represented as a floating box showing the mean and range with scores for Patient X (blue) and Y (red) superimposed. (I) K_{rad}/K_{FA} ratio in the periventricular, deep and subcortical WM for Patient X (blue), patient Y (red) and age-matched controls (black). (J) K_{rad}/K_{FA} ratio in cohort of patients with PKU (red) vs. controls (black). The K_{rad}/K_{FA} ratio for patients with PKU was higher than control at periventricular, deep and pericortical levels (****$p < 0.001$). Error bars indicate mean ± standard deviation.

gliobastoma model (Rocha and Martins, 2012), and was recently described as the most diagnostically efficient measure of cerebral damage in a longitudinal clinical study of carbon monoxide poisoning (Schoemans et al., 2010).

In this present work, diffusion and DKI metric differences were generally greater in the periventricular WM than deep or pericortical WM, supporting our hypothesis that WM abnormalities would radiate outward from the ventricles. We constructed a simple biomarker ratio comprising the K_{rad} and K_{FA} metrics to capture these progressive changes. In Patients X and Y this K_{rad}/K_{FA} ratio highlighted this effect, and our Replication analysis significantly delineated a mixed-severity PKU cohort from control subjects throughout the periventricular, deep and pericortical WM compartments. The presence of mild PKU subjects was likely reflected in the less pronounced differences in pericortical WM, however the fact that this ratio could detect WM pathology in normal-appearing WM, and reveal WM change even in the least-affected pericortical WM is encouraging. We hypothesise that this ratio – or a similar approach reflecting distribution of kurtotic changes – may be a novel biomarker for PKU.

In our study K_{rad}/K_{FA} did not correlate with lifetime mean Phe, but did correlate with more recent concentrations. Future work is needed to establish the relationship between DKI metrics and Phe levels. Although Phe is the gold standard for assessing disease status and dietary treatment efficacy, Phe levels represent control only over a period of days, with frequent sampling required to understand long-term control. Our results suggest that the K_{rad}/K_{FA} ratio is sensitive to dietary control over the medium term. If confirmed in larger subsequent studies, this metric may allow more meaningful clinical monitoring than infrequent Phe alone. This seems particularly important in adults, a significant number of whom are poorly compliant with regular Phe level monitoring.

Relationships between cognitive dysfunction and WM pathology are poorly understood in PKU, as are the downstream biological consequences of elevated Phe. While some authors have found that Phe directly affects oligodendrocytes and myelin, impairing synaptic plasticity, neurotransmission and bioenergetics (Antenor-Dorsey et al., 2013), others have found no such relationship [52], implying that there may be under-recognised Phe-independent methods of myelination. Our study did not find group-based differences in attention scores overall; we found that the K_{rad}/K_{FA} ratio negatively correlated with measures of attention, with particular impairment in patients with highest K_{rad}/K_{FA} ratios. This leads us to hypothesise that there may be an interplay between pathology measured by DKI metrics and attentional dysfunction, however further work is needed to investigate this.

Broad interpretation of our findings is limited by several factors. Our study design focused on two well-characterised siblings, with further validation in a modest PKU cohort. Due to the cross-sectional nature of our study, we were unable to demonstrate presumed longitudinal changes in our metrics. Phe levels were not available during the teenage years for Patients X and Y, limiting inference of Phe-related changes over time. Similarly, lifetime Phe monitoring in the PKU cohort was not homogeneous. Confirmation via larger longitudinal study, and testing of relationships between diffusion MRI/DKI metrics, Phe levels and cognition are key areas for future research.

In conclusion, we present the first application of DKI in PKU and demonstrate that WM diffusion kurtosis alterations are present. These abnormalities may be greater in proximity to the ventricles and

heightened with reduced diet compliance and increased Phe levels. That this is detectable in PKU even without conspicuous clinical manifestations suggests a future role in longitudinal monitoring.

Funding

This work was funded by the NSW PKU Association. SMG acknowledges the support of the Heart Research Institute, Sydney Medical School, the Frecker Family, and the Parker-Hughes Bequest.

CRediT authorship contribution statement

Sarah C. Hellewell: Conceptualization, Methodology, Data curation, Formal analysis, Writing - review & editing. **Thomas Welton:** Conceptualization, Methodology, Data curation, Formal analysis. **Kate Eisenhuth:** Methodology, Data curation, Writing - review & editing. **Michel C. Tchan:** Conceptualization, Methodology, Data curation, Formal analysis, Writing - review & editing. **Stuart M. Grieve:** Conceptualization, Methodology, Formal analysis, Writing - review & editing.

Conflict of Interest

Sarah C. Hellewell, Thomas Welton, Kate Eisenhuth, Michel C. Tchan and Stuart M. Grieve declare that they have no conflict of interest.

Appendix A. Supplementary data

Supplementary data to this article can be found online at https://doi.org/10.1016/j.nicl.2020.102555.

References

Anderson, P.J., Leuzzi, V., 2010. White matter pathology in phenylketonuria. Mol. Genet. Metab. 99 (Suppl 1), S3–9.
Antenor-Dorsey, J.A., Hershey, T., Rutlin, J., et al., 2013. White matter integrity and executive abilities in individuals with phenylketonuria. Mol. Genet. Metab. 109 (2), 125–131.
Arab, A., Wojna-Pelczar, A., Khairnar, A., Szabo, N., Ruda-Kucerova, J., 2018. Principles of diffusion kurtosis imaging and its role in early diagnosis of neurodegenerative disorders. Brain Res. Bull. 139, 91–98.
Bick, U., Ullrich, K., Stober, U., et al., 1993. White matter abnormalities in patients with treated hyperphenylalaninaemia: Magnetic resonance relaxometry and proton spectroscopy findings. Eur. J. Pediatr. 152 (12), 1012–1020.
Blau, N., van Spronsen, F.J., Levy, H.L., 2010. Phenylketonuria. Lancet 376 (9750), 1417–1427.
Christ, S.E., Huijbregts, S.C., de Sonneville, L.M., White, D.A., 2010. Executive function in early-treated phenylketonuria: profile and underlying mechanisms. Mol. Genet. Metab. 99 (Suppl 1), S22–32.
Chuhutin, A., Hansen, B., Wlodarczyk, A., Owens, T., Shemesh, N., Jespersen, S.N., 2020. Diffusion Kurtosis imaging maps neural damage in the EAE model of multiple sclerosis. NeuroImage 208, 116406.
Deon, M., Sitta, A., Faverzani, J.L., et al., 2015. Urinary biomarkers of oxidative stress and plasmatic inflammatory profile in phenylketonuric treated patients. Int. J. Dev. Neurosci. 47, 259–265.
Dezortova, M., Hajek, M., Tintera, J., Hejcmanova, L., Sykova, E., 2001. MR in phenylketonuria-related brain lesions. Acta Radiol. 42 (5), 459–466.
Ding, X.Q., Fiehler, J., Kohlschutter, B., et al., 2008. MRI abnormalities in normal-appearing brain tissue of treated adult PKU patients. J. Magn. Reson. Imaging 27 (5), 998–1004.
Ding, X.Q., Fiehler, J., Kohlschütter, B., et al., 2008. MRI abnormalities in normal-appearing brain tissue of treated adult PKU patients. J. Magn. Resonance Imaging Off. J. Int. Soc. Magn. Resonance Med. 27 (5), 998–1004.
Dyer, C.A., 1999. Pathophysiology of phenylketonuria. Mental Retardation Dev. Disabilities Res. Rev. 5 (2), 104–112.
Enns, G.M., Koch, R., Brumm, V., Blakely, E., Suter, R., Jurecki, E., 2010. Suboptimal outcomes in patients with PKU treated early with diet alone: revisiting the evidence. Mol. Genet. Metab. 101 (2–3), 99–109.
Falangola, M.F., Guilfoyle, D.N., Tabesh, A., et al., 2014. Histological correlation of diffusional kurtosis and white matter modeling metrics in cuprizone-induced corpus callosum demyelination. NMR Biomed. 27 (8), 948–957.
Fischl, B., 2012. FreeSurfer. *NeuroImage.* 62 (2), 774–781.
González, M.J., Polo, M.R., Ripollés, P., et al., 2018. White matter microstructural damage in early treated phenylketonuric patients. Orph. J. Rare Dis. 13 (1), 188.
Greve, D.N., Fischl, B., 2009. Accurate and robust brain image alignment using boundary-based registration. NeuroImage. 48 (1), 63–72.
Hansen, B., 2019. An introduction to Kurtosis fractional anisotropy. AJNR Am. J. Neuroradiol. 40 (10), 1638–1641.
Hansen, B., Jespersen, S.N., 2016. Kurtosis fractional anisotropy, its contrast and estimation by proxy. Sci. Rep. 6, 23999.
Hofman, D.L., Champ, C.L., Lawton, C.L., Henderson, M., Dye, L., 2018. A systematic review of cognitive functioning in early treated adults with phenylketonuria. Orph. J. Rare Dis. 13 (1), 150.
Hood, A., Grange, D.K., Christ, S.E., Steiner, R., White, D.A., 2014. Variability in phenylalanine control predicts IQ and executive abilities in children with phenylketonuria. Mol. Genet. Metab. 111 (4), 445–451.
Huijbregts, S.C., de Sonneville, L.M., van Spronsen, F.J., Licht, R., Sergeant, J.A., 2002. The neuropsychological profile of early and continuously treated phenylketonuria: Orienting, vigilance, and maintenance versus manipulation-functions of working memory. Neurosci. Biobehav. Rev. 26 (6), 697–712.
Inwood, A.C., Lewis, K., Balasubramaniam, S., et al. Australasian consensis guidelines for the management of phenylketonuria (PKU) throughout the lifespan. 2017.
Jelescu, I.O., Zurek, M., Winters, K.V., et al., 2016. In vivo quantification of demyelination and recovery using compartment-specific diffusion MRI metrics validated by electron microscopy. NeuroImage 132, 104–114.
Jones, D.K., Horsfield, M.A., Simmons, A., 1999. Optimal strategies for measuring diffusion in anisotropic systems by magnetic resonance imaging. Magn. Reson. Med. 42 (3), 515–525.
Kakulas, B.A., Hamilton, G.J., Mastaglia, F.L., 1968. Clinical and neuropathological observations in phenylketonuria. Proc Aust Assoc Neurol. 5 (1), 155–158.
Kelm, N.D., West, K.L., Carson, R.P., Gochberg, D.F., Ess, K.C., Does, M.D., 2016. Evaluation of diffusion kurtosis imaging in ex vivo hypomyelinated mouse brains. NeuroImage 124 (Pt A), 612–626.
Kienzle Hagen, M.E., Pederzolli, C.D., Sgaravatti, A.M., et al., 2002. Experimental hyperphenylalaninemia provokes oxidative stress in rat brain. *Biochimica et Biophysica Acta (BBA)*. Mol. Basis Dis. 1586 (3), 344–352.
Koch, R.K., 1999. Issues in newborn screening for phenylketonuria. Am. Fam. Physician 60 (5), 1462–1466.
Lesbats, C., Kelly, C.L., Czanner, G., Poptani, H., 2020. Diffusion kurtosis imaging for characterizing tumor heterogeneity in an intracranial rat glioblastoma model. NMR Biomed. 33 (11), e4386.
Leuzzi, V., Tosetti, M., Montanaro, D., et al., 2007. The pathogenesis of the white matter abnormalities in phenylketonuria. A multimodal 3.0 tesla MRI and magnetic resonance spectroscopy (1H MRS) study. J. Inherit. Metab. Dis. 30 (2), 209–216.
Malamud, N., 1966. Neuropathology of phenylketonuria. J. Neuropathol. Exp. Neurol. 25 (2), 254–268.
Maller, J.J., Welton, T., Middione, M., Callaghan, F.M., Rosenfeld, J.V., Grieve, S.M., 2019. Revealing the Hippocampal Connectome through super-resolution 1150-direction diffusion MRI. Sci. Rep. 9 (1), 2418.
Nardecchia, F., Manti, F., Chiarotti, F., Carducci, C., Carducci, C., Leuzzi, V., 2015. Neurocognitive and neuroimaging outcome of early treated young adult PKU patients: A longitudinal study. Mol. Genet. Metab. 115 (2–3), 84–90.
Pearsen, K.D., Gean-Marton, A.D., Levy, H.L., Davis, K.R., 1990. Phenylketonuria: MR imaging of the brain with clinical correlation. Radiology 177 (2), 437–440.
Rocha, J.C., Martins, M.J., 2012. Oxidative stress in phenylketonuria: future directions. J. Inherit. Metab. Dis. 35 (3), 381–398.
Romani, C., Palermo, L., MacDonald, A., Limback, E., Hall, S.K., Geberhiwot, T., 2017. The impact of phenylalanine levels on cognitive outcomes in adults with phenylketonuria: Effects across tasks and developmental stages. Neuropsychology 31 (3), 242–254.
Romani, C., Manti, F., Nardecchia, F., et al., 2019. Adult cognitive outcomes in phenylketonuria: explaining causes of variability beyond average Phe levels. Orphanet J. Rare Dis. 14 (1), 273.
Schoemans, R., Aigrot, M.-S., Wu, C., et al., 2010. Oligodendrocyte development and myelinogenesis are not impaired by high concentrations of phenylalanine or its metabolites. J. Inherit. Metab. Dis. 33 (2), 113–120.
Silverstein, S.M., Berten, S., Olson, P., et al., 2007. Development and validation of a World-Wide-Web-based neurocognitive assessment battery: WebNeuro. Behav. Res. Methods 39 (4), 940–949.
Steven, A.J., Zhuo, J., Melhem, E.R., 2014. Diffusion kurtosis imaging: an emerging technique for evaluating the microstructural environment of the brain. AJR Am. J. Roentgenol. 202 (1), W26–33.
Tabesh, A., Jensen, J.H., Ardekani, B.A., Helpern, J.A., 2011. Estimation of tensors and tensor-derived measures in diffusional kurtosis imaging. Magn. Reson. Med. 65 (3), 823–836.
Taylor, E.H., Hommes, F.A., 1983. Effect of experimental hyperphenylalaninemia on myelin metabolism at later stages of brain development. Int. J. Neurosci. 20 (3–4).
Trefz, F.K., van Spronsen, F.J., MacDonald, A., et al., 2015. Management of adult patients with phenylketonuria: Survey results from 24 countries. Eur. J. Pediatr. 174 (1), 119–127.
Ullrich, K., Moller, H., Weglage, J., et al., 1994. White matter abnormalities in phenylketonuria: Results of magnetic resonance measurements. Acta Paediatr. Suppl. 407, 78–82.
Vermathen, P., Robert-Tissot, L., Pietz, J., Lutz, T., Boesch, C., Kreis, R., 2007. Characterization of white matter alterations in phenylketonuria by magnetic resonance relaxometry and diffusion tensor imaging. Magn. Reson. Med. 58 (6), 1145–1156.
Weglage, J., Fromm, J., van Teeffelen-Heithoff, A., et al., 2013. Neurocognitive functioning in adults with phenylketonuria: results of a long term study. Mol. Genet. Metab. 110 (Suppl), S44–48.

Williams, R.A., Mamotte, C.D.S., Burnett, J.R., 2008. Phenylketonuria: An inborn error of phenylalanine metabolism. Clin. Biochem. Rev. 29 (1), 31–41.
Zhang, Y., Brady, M., Smith, S., 2001. Segmentation of brain MR images through a hidden Markov random field model and the expectation-maximization algorithm. IEEE Trans. Med. Imaging 20 (1), 45–57.
Zhang, Y., Wang, T., Lei, J., et al., 2019. Cerebral damage after carbon monoxide poisoning: A longitudinal diffusional Kurtosis imaging study. AJNR Am. J. Neuroradiol. 40 (10), 1630–1637.